Experiments and simulations of the humidity dependence of friction between nanoasperities and graphite: The role of interfacial contact quality

Kathryn Hasz, Zhijiang Ye, Ashlie Martini, and Robert W. Carpick

Phys. Rev. Materials **2**, 126001 — Published 7 December 2018

DOI: 10.1103/PhysRevMaterials.2.126001

Experiments and Simulations of the Humidity Dependence of Friction between Nanoasperities and Graphite: The Role of Interfacial Contact Quality

Kathryn Hasz[1,5], Zhijiang Ye[2,5], Ashlie Martini[3], Robert W. Carpick[4,*]

1 *Department of Materials Science and Engineering, University of Pennsylvania, 3231 Walnut Street, Philadelphia, Pennsylvania, 19104, United States*

2 *Department of Mechanical and Manufacturing Engineering, Miami University, 650 E. High Street, Oxford, Ohio 45056, United States*

3 *Department of Mechanical Engineering, University of California Merced, 5200 North Lake Road, Merced, California 95343, United States*

4 *Department of Mechanical Engineering and Applied Mechanics, University of Pennsylvania, 220S. 33rd Street, Philadelphia, Pennsylvania 19104, USA*

5 *Contributed equally to this work*

Abstract:

We use atomic force microscopy and Grand Canonical Monte Carlo atomistic simulations to study stick-slip friction of tetrahedral amorphous carbon (ta-C) probes sliding against highly oriented pyrolytic graphite (HOPG) at relative humidities ranging from <1% to near saturation. Friction varies with humidity in a non-monotonic manner such that water acts as a lubricant only above a threshold humidity; below that threshold, water increases friction substantially relative to dry sliding. Adhesion forces also show a similar non-monotonic behavior. A non-monotonic dependence of friction and adhesion on humidity for single asperity interfaces has previously

been attributed to the humidity-dependent adhesion force due to the water meniscus that forms at the contact, which is presumed to increase the solid-solid contact area. However, our simulations show no such increase in solid-solid contact area, but do show a small, continuous increase in tip-sample separation as humidity increases. Experimentally, no significant change in lateral stiffness is observed with humidity. All of this contradicts the hypothesis that the friction increase is due to capillary adhesion increasing the contact area. We show that water molecules are present between the tip and sample in increasing numbers as the humidity increases. From this, we attribute the non-monotonic friction trend to the changing quality of the contact between the water and the substrate, quantified by the number of water molecules in the interface and their registry with the HOPG surface atoms, which in simulations also shows a non-monotonic trend with humidity. Hysteresis observed in the variation of friction with humidity in both experiments and simulations is explained by the larger energy barrier for surface desorption of water molecules compared to adsorption.

I. Introduction

The friction force between any two surfaces can depend strongly on environmental conditions, which include temperature, pressure, surrounding gas composition, and relative humidity[1,2]. Environment is particularly consequential for solid lubricants, where consistently low friction across a range of operating conditions is desirable. For example, macroscale experiments have shown that molybdenum disulfide (MoS_2) has very low friction in vacuum and dry conditions but not at higher humidities[3,4], while graphite and diamond have low friction in humid environments, but not in dry conditions[5–13]. These materials are therefore good solid lubricants only as long as the low friction environment is maintained. Because of these

limitations, MoS_2 is commonly used in systems functioning in vacuum or outer space, while graphite is common when a solid lubricant is needed in terrestrial applications.

While there exists an understanding of the origins of the humidity dependence for these and other solid lubricants at the macroscale, the nanoscale mechanisms behind the humidity dependence of solid lubricant friction are not well understood. Previous experiments and simulations have shown that humidity can affect both nanoscale adhesion and friction[2, 14–31]. For example, nanoscale adhesion, measured between atomic force microscopy (AFM) tips and various substrates, has been repeatedly found to increase as the humidity increases from low to moderate levels. In some cases, only an increase is seen[15,16], while in other cases, a non-monotonic trend of an increase followed by a decrease above intermediate humidity values is observed[18–22]. Some reports of monotonic trends appear due to a limited humidity range used in the measurements. The non-monotonic behavior is attributed to the competing effects of an increasing meniscus size with decreasing Laplace pressure in the meniscus as the humidity increases, producing a maximum in the adhesive force[18-20], which is discussed further below.

Previous studies of humidity effects on nanoscale friction have also shown a non-monotonic trend similar to that seen for adhesion[14,23-26]. For a silicon tip on hydrophilic CrN, this trend was observed and attributed to capillary forces from water bridges developed in a multiasperity contact[23]. For a silicon tip sliding on silicon (with native oxides present), an increase in friction in humid air was attributed to the formation of a capillary, where it was assumed that the resulting Laplace pressure increased adhesion and led to growth of the solid-solid contact area[14]. Friction was seen to decrease as the pressure was reduced from atmosphere to ultrahigh vacuum in a silicon on silicon system, also attributed to the decrease in capillary size as water was pumped out of the system[31]. A strong non-monotonic trend was seen for a silicon

tip sliding on muscovite mica, with a weak or flat trend seen for the same tip sliding on an Al_2O_3 substrate or MoS_2 layers on either the mica or Al_2O_3. This was attributed to the adsorption of an additional water layer on the hydrophilic mica that increased the Laplace pressure at moderate humidites[26]. The hydrophobicity of the surface was seen to influence friction for a silicon tip sliding on ZnO surfaces[25]. The two ZnO surfaces were treated to attain different degrees of hydrophobicity. The more hydrophilic surface had higher friction at humidities ranging from 3-26%, thought to come from increased wetting and a stronger, solid-like meniscus due to increased wettability of the hydrophilic surface[32]; friction was equivalent for both surfaces above 40%. Indentation experiments also measured a more solid-like behavior of the meniscus on the hydrophilic substrate. The effect disappeared at high humidities, where the amount of water present lessened the effect of Laplace pressure, and the non-monotonic trend was seen on both hydrophobic and hydrophilic surfaces. One report suggests that, on graphite, an ice-like layer forms, with different thicknesses as humidity changes; rupture of that bridge controlling the friction behavior[22]. Others have seen a similar ice-like layer form on clean graphene in MD simulations [33]. While these studies explored how the water present and the capillary formed can increase friction and adhesion, the humidity dependence of the interfacial contact *quality* - how much the interfacial atoms are at energetically favorable positions - remains unexplored. Contact quality can be considered as a physically-motivated description of the interfacial shear strength τ, with interfacial static friction F depending on contact area A via $F = \tau A$ [34]. Recently it was shown in simulations that increased contact quality, as measured by the strength of interactions between the atoms of a silicon tip and a graphene sample, strongly increased friction [35] in agreement with experiments [34]. This suggests that combining experiments and complementary atomistic

simulations can enable us to probe the frictional behavior of a buried interface as it evolves with humidity.

Overall, the humidity dependence of atomic-scale friction is a complex aspect of frictional sliding that is not well understood, is sensitive to multiple experimental parameters, and is attributable to multiple mechanisms. In this study, we probe the mechanisms behind the humidity dependence of atomic friction between tetrahedral amorphous carbon (ta-C) coated tips and highly oriented pyrolytic graphite (HOPG) using AFM measurements and corresponding Grand Canonical Monte Carlo (GCMC) simulations. We investigate atomic-scale friction under a wide range of relative humidities (RH), from 0-100% in simulations and <1-80% in experiments. We perform studies by both ramping up and ramping down the humidity, and by randomly varying the humidity. For the first time, atomic stick-slip motion is resolved at every humidity level in the experiments, and a previously unreported hysteretic friction behavior is observed between ramping up and ramping down the humidity in both experiments and simulations. Our experiments reveal the humidity-dependence of stick-slip friction, and the matched GCMC simulations are used to explore the mechanisms that underlie the behavior seen experimentally. Specifically, the simulations enable investigation of the roles of the previously proposed mechanisms of the non-monotonic trend: water absorption on surface, water meniscus formation between the tip and substrate, and formation of a thin ice-like water film. The atomic details obtained from simulations are also used to explore the mechanisms underlying the observed friction hysteresis.

II. Methods

A. Experiments

Experiments were conducted in an RHK 350 AFM (RHK Technology Inc.) to investigate the humidity dependence of the friction force between a tetrahedral amorphous carbon (ta-C)-coated tip (~70% of sp^3 bonded carbon) (ContDLC, Budget Sensors, Sofia, Bulgaria) and a highly ordered pyrolytic graphite (HOPG) substrate. The HOPG sample (SPI-1, SPI Supplies, West Chester, PA, USA) was freshly exfoliated using mechanical exfoliation before measurements and placed in the measurement chamber within 10 minutes of exfoliation. The chamber was then pumped down to 10^{-5} Torr, and the sample was heated to 150 °C and held there for one hour to substantially remove adsorbed contaminants (such as adventitious hydrocarbons and water) from the surface and achieve clean graphite, which is hydrophilic[32,36-37]. Annealing is conducted in vacuum to avoid oxidation or other surface chemical reactions. Once the sample was cooled back to room temperature, the chamber was backfilled with pure dry nitrogen from the vapor of a liquid nitrogen dewar. We introduced water vapor by bubbling nitrogen gas from the same source through deionized water. The humidity was controlled by varying the ratio of dry nitrogen and humid nitrogen gas flowed through the chamber. We achieved stable relative humidities between <1% and 80%. The humidity in the chamber was measured with a hygrometer (Fisher).

Two different ta-C-coated cantilever probes with integrated tips were used. The first cantilever (tip 1) had a normal spring constant of 2.1 ± 0.3 N/m and a lateral spring constant of 24.7 ± 0.4 N/m; the second (tip 2) had a normal spring constant of 0.323 ± 0.007 N/m and a lateral spring constant of 7.5 ± 0.5 N/m. Spring constants were measured by the Sader method, with assumed uniformity of the photodiode sensitivity for normal and lateral deflections[38-39]. The variations in spring constants between the cantilevers is likely from the difference in cantilever width. The tip radii were estimated to be 42 ± 15 nm and 65 ± 17 nm, respectively, and

confirmed to be unchanged throughout the experiment within uncertainty, by using blind tip reconstruction on a sample of ultrananocrystalline diamond at each humidity level (see Figure S-1)[40-41].

Measurements were performed at zero externally applied load, held approximately constant using normal force feedback, but with a low time constant to prevent the feedback from responding to atomic-scale deflections of the cantilever during stick-slip motion. Adhesion forces were found to be 6 ± 2 nN for tip 1 and 3 ± 2 nN for tip 2 at <1% relative humidity based on several tens of force-distance curve measurements. Frequent force-distance curve measurements allowed for regular correction of any thermal drift in the position of the laser on the photodiode and to verify continued operation at zero externally applied load in case adhesion forces changed. All measurements were obtained at room temperature, atmospheric pressure, and with three scan speeds: 17 nm/s, 33 nm/s, and 67 nm/s; the scan rate was held constant at 300 lines/s, with the scan size varied from 5x5 to 10x10 to 20x20 nm^2 respectively. No trend was resolved with changing speed over this range. Friction data reported are the average friction force over the scanned area used for each scan speed (*i.e.*, scan area). Measurements at different humidities were obtained both at the same location and at fresh locations. No difference was seen between measurements obtained at previously scanned vs freshly scanned locations, thus ensuring that scanning was not modifying the sample or the tip in any systematic way. Atomic-lattice stick slip motion was obtained for all measurements, as seen in a typical scan in Figure 1a,b and Figure S-2 [42]. The lattice has threefold symmetry with a period of 0.244 ± 0.005 nm; the lattice spacing of the graphite(0001) surface is 0.246 nm. Experiments were performed by ramping up and then ramping down the humidity in intervals of 20%, and also by randomly

varying the humidity with intermediate vacuum anneals at 150 °C for 1 hour to eliminate any history-dependent water adsorption effects.

Some images showed evidence of surface inhomogeneity (see Figure S-3)[42], yet atomic stick-slip was observable despite this. The occurrence of tilting and localized changes in friction loops like those reported by Jinesh and Frenken[28,29] was considered, but no evidence for this was observed in experiments.

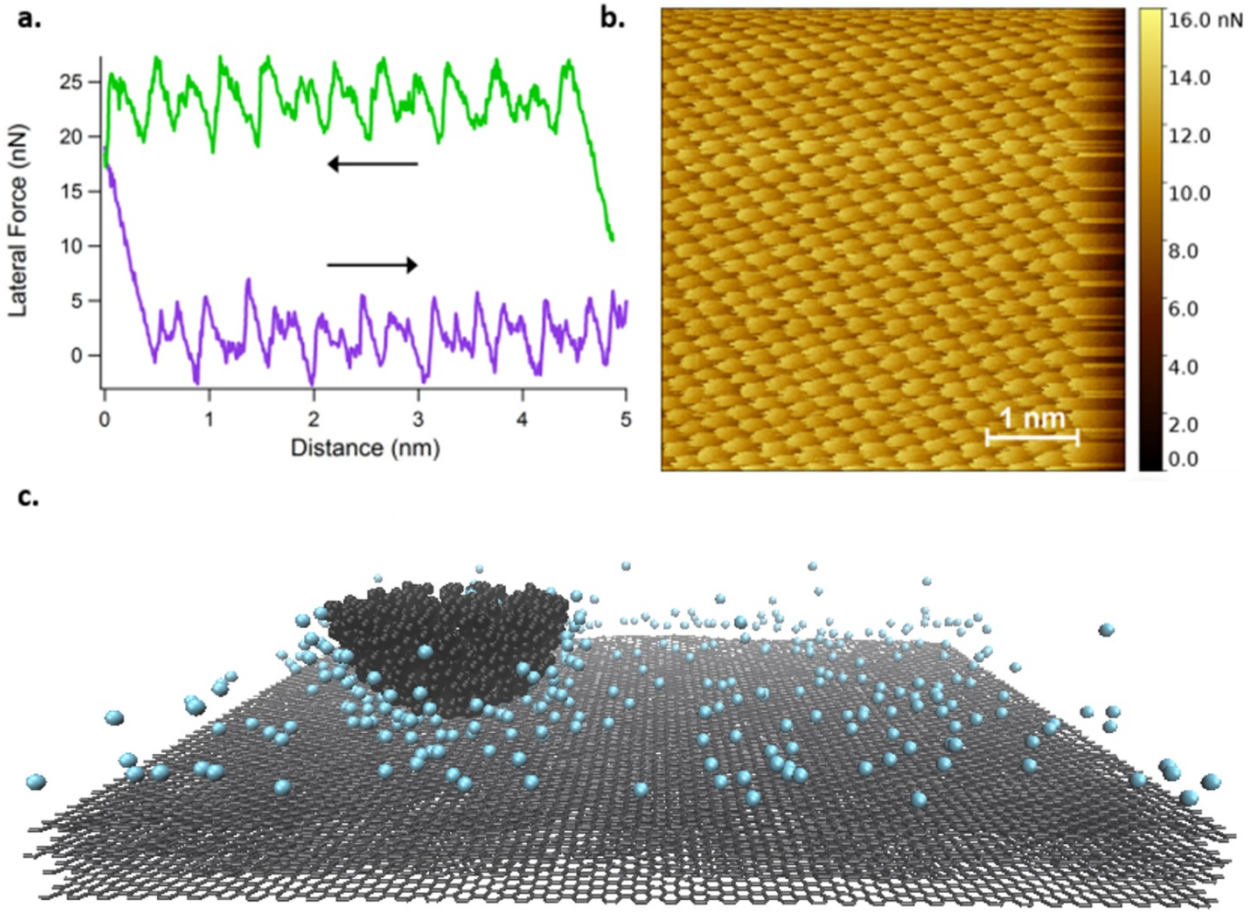

Figure 1: (a) Representative experimental friction loop on HOPG with clear stick slip pattern taken at 40% RH. (b) Experimental AFM lateral force image with clear six-fold symmetry of HOPG. (c) Snapshots of the GCMC simulations of a ta-C coated AFM tip apex, shown in black,

sliding on a model graphite surface, shown in gray, at 20% relative humidity. The blue spheres represent individual coarse-grained water molecules.

B. Simulations

The atomistic model consisted of the apex of a ta-C AFM tip placed on a three-layer graphite substrate as illustrated in Figure 1c. The graphite substrate had dimensions of 16×10 nm^2 (the longer direction corresponded to the sliding direction); the positions of the atoms in the bottom graphite layer were fixed. While strictly speaking the simulated sample is three-layer graphene and not graphite, AFM experiments have shown that 3-layer graphene exhibits nearly equivalent frictional behavior as graphite [35,49]. Moreover, layer-dependent effects reported for graphene are suppressed when graphene is supported by adherent flat substrates[49]; thus, the use of 3 layers here with the bottom layer fixed is sufficiently representative of graphite. Following an established procedure[50], the ta-C tip apex was formed by heating a block of crystalline diamond to 8000 K, quenching it back to room temperature within 1 ns, and then cutting the hemispherical shape (2.5 nm radius) from the resulting block of amorphous carbon. The resulting tip contained ~60% of sp^3 bonded carbon, consistent with the manufacturer's estimate of sp^3 carbon in the experimental tips. The topmost atoms in the tip were treated as a rigid body that was connected by a harmonic spring to a support that moved laterally[43] at a constant speed of 1 m/s. The spring had a stiffness of 8 N/m in the horizontal directions, giving a similar stiffness to the experiments, but did not resist motion in the vertical direction (normal to the graphite surface). Simulations were performed with zero applied load. A Langevin thermostat was applied to all unconstrained atoms to maintain a temperature of 300 K. The water molecules were treated using the single molecule coarse-grained "monatomic water" (mW) model of Molinero and Moore[44, 60] (details can be found in SI)[42]. The mW model was show to accurately reproduce

the density, structure and energetics of water but with much lower computational cost than full atomistic models[44, 60]. In addition, the current GCMC command in LAMMPS only allows one chemical potential input for a specific molecule, meaning that coarse-grained water enables its use. The inter-atomic interactions within the tip and substrate were described via the Adaptive Intermolecular Reactive Empirical Bond Order (AIREBO)[45] potentials, and the long-range interactions between tip, water and substrate were modeled using the Lennard-Jones (LJ) potential (details can be found in SI)[42].

The relative humidity, defined as the ratio of the partial pressure of water vapor to the saturation vapor pressure of water, was controlled using the water chemical potential[46] in our GCMC simulations through following equation:

$$\mu = \mu^{\circ} + RT \ln \frac{P}{P^{\circ}}, \quad (1)$$

where μ is the desired chemical potential, μ° is the chemical potential at room temperature, R is the ideal gas constant, T is temperature, P is the partial pressure of water vapor, and P° is the saturation vapor pressure. We varied chemical potential to simulate relative humidity from 0% to 100%. The humidity started at 0%, was increased to 100%, and then decreased again to 0% to follow the same procedure as the experiments. At each relative humidity, we started sliding the tip after the system reached a steady state where the number of water molecules fluctuated about a constant value (see Figure S-4)[42].

All the simulations were performed using GCMC with LAMMPS simulation software[47]. Simulated friction traces are shown in Figure S-5[42].

III. Results and Discussion

Figure 2 shows the experimental friction force for a ta-C AFM tip sliding on the HOPG surface, and Figure 3a shows the results from simulations. In both simulations and experiments, the normal load is held constant. Both show a non-monotonic dependence of the friction force on the humidity: friction first increases and then decreases as the relative humidity increases from <1% to 100%, with a peak value of friction between 40% and 60% relative humidity in experiments and between 60% and 80% in the simulations. This non-monotonic humidity-dependent friction behavior indicates that water only acts as a lubricant above a threshold humidity; below this threshold humidity, friction increases strongly with increasing humidity. Compared with the friction force values at low humidity, the friction force at the peak increases three-fold in the experiments and six-fold in the simulations. Experimental data were acquired with two tips. The magnitude of the friction force varies between the two AFM tips, likely due to specific tip attributes including its precise size, geometry, and surface chemistry, but the overall shape of the friction-humidity plot remains the same within the experimental scatter (data from the second tip are shown in Fig. S-6)[42]. Although nanoscale friction has been seen to vary with speed depending on the humidity (for silica-silica contacts)[23], no consistent trend with the three speeds used here is seen, likely due to the relatively small range of velocities tested (less than an order of magnitude).

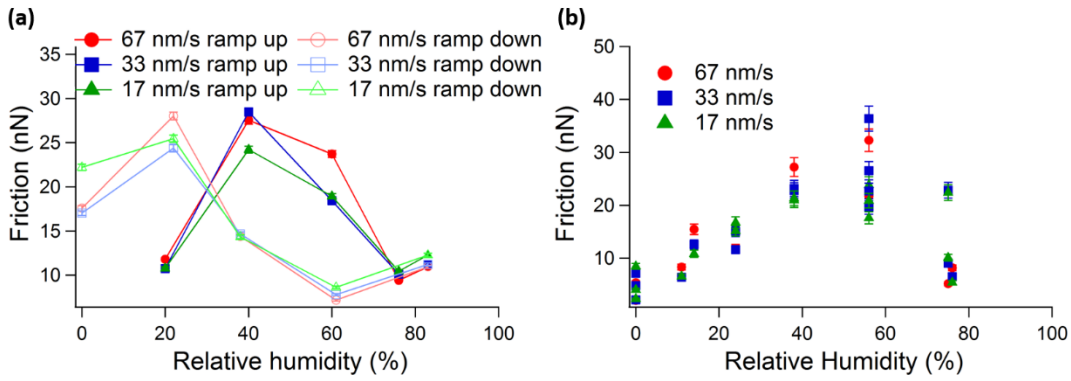

Figure 2: Friction vs. relative humidity for a ta-C tip sliding on a HOPG sample. (a) Experimental results obtained with successively increasing ("ramp up") and then decreasing ("ramp down") humidities with tip 1, and (b) experimental results with periodic sample annealing between each change in humidity with tip 2; no connecting line is shown since the humidity was varied randomly. In both cases, friction has a maximum value at intermediate humidities, with the hysteresis occurring in (a). Three sliding speeds were used at each humidity, as indicated.

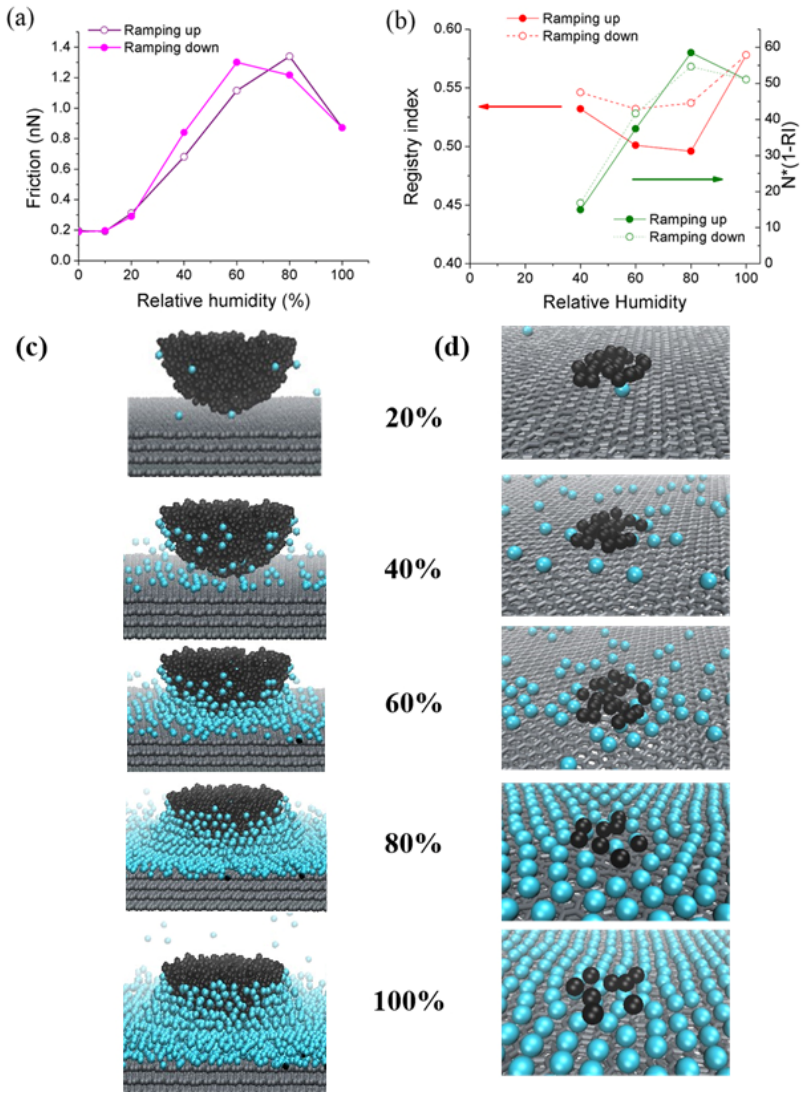

Figure 3: (a) Friction vs. relative humidity for a ta-C tip sliding on HOPG from GCMC simulations. (b) Average registry index (RI) of the near-tip water molecules relative to the graphite substrate (dashed red and orange lines), and a combined measure of the number and registry of the water molecules on the graphite, quantified by (N) multiplied by (1-RI) (solid light green and dark green lines). (c,d) Snapshots of the tip and meniscus (c) and the tip atoms and water molecules on the surface (d) at 20%-100% RH.

We now consider how the non-monotonic friction behavior relates to the level of water coverage on the HOPG surface, the formation of a capillary between the tip and sample, and the quality of the contact at different humidities. Since the presence of water strongly affects the interactions between the tip and sample, we consider the contact quality based on the water-graphite interactions. At low relative humidities, friction is small, as shown in Figure 2 and Figure 3a. The interactions are primarily determined by the van der Waals interactions between the ta-C and HOPG, as would be the case in dry frictional sliding[18]. The simulations show very few water molecules present between the tip and the sample at 40% RH or below, as seen in Figure 3c,d, where the black spheres are tip atoms located within 0.5 nm of the substrate. The contact quality is in part characterized by the registry index (RI)[48], a parameter ranging from 0 to 1, where 0 corresponds to the most energetically favorable location of an atom or molecule on a substrate, water on graphite in our case, and 1 corresponds to the most energetically unfavorable location (more details are in the SI)[42]. We only include the water molecules at contact for RI calculation since there are very few tip atoms in contact with substrate. Note that we calculate time average number of water molecules in contact over the whole sliding period. This parameter calculated for the positions of the water relative to the substrate is shown in Figure 3b. It is observed that quality of contact is low, i.e. there are very few water molecules with a low RI. Molecules with low RI can act as pinning sites, i.e. molecules in energetically favorable locations between the tip and substrate can resist sliding motion.

As the humidity increases, more adsorbed water is present on both tip and substrate surfaces, and at the interface between them. From this, a meniscus forms between the tip and substrate. Due to fluctuations of the water molecules in the nanoscale volume of the tip-sample contact region, a clear representation of the meniscus from the simulations is more fully captured

by time-averaging the water molecule positions as opposed to viewing a single snapshot like those in Figure 3. Figures 4a and b show time-averaged water density profiles between tip and substrate at 40 and 80% RH and clearly demonstrate that a water meniscus starts to form and grow as the humidity increases.

Previously, increased friction with humidity was attributed to the water meniscus applying additional capillary force[14,17,24, 28-29]. From the Young-Laplace equation, the overall negative curvature of the meniscus leads to a negative Laplace pressure (lower pressure inside vs. outside the liquid), proportional to the surface tension of water and the inverse of the meniscus radius[24]. As the meniscus exerts less pressure on the tip and sample than the surrounding environment, a net force pushes the tip and sample together, effectively acting as an additional load, thus increasing contact area and friction. This load can be estimated by multiplying the Laplace pressure by the meniscus cross-sectional area. Initially, the rapid growth of meniscus cross-sectional outpaces the decrease in Laplace pressure due to the growing meniscus radius, so the net force should increase. As the meniscus grows further, the meniscus area should saturate while the Laplace pressure continues to drop. The capillary force thus decreases until the contact is fully flooded, at which point the capillary force disappears[24].

While this model for the non-monotonic dependence of the meniscus force may have some effect on friction, our results indicate it is not the dominant factor. We do see a non-monotonic trend in adhesion in our experiments (see Figure S-7)[42] However, a change in contact area normally would alter the lateral stiffness of the contact[62]; as shown in Fig S-8[42], the lateral stiffness for each tip is constant within measurement error across all humidities, with <10% of the measurements outliers with no systematic trend. Furthermore, in the simulations, there is no increase in tip-sample contact area as a function of humidity. Instead, the solid-solid contact

between tip and sample actually decreases with increasing humidity as water infiltrates that space, as seen in Figure 3d by the decreasing number of tip atoms within 0.5 nm of the surface. Figure 4c shows the vertical distance between tip and substrate at different humidities from the simulations. At 0% RH, it has the smallest vertical distance, as there are no water molecules between the tip and sample and the tip is directly in contact with the sample. Above 20% RH, the gap increases as the number of water molecules between the tip and substrate increases. This means that there is not an increase in tip-substrate contact area, as previously proposed[25]. In fact, the solid-solid contact between the tip and substrate decreases as water intercalates between the tip and sample, as seen by the clear ~0.1 nm increase in the vertical distance between tip and sample as humidity increases (from 0.37 to 0.48 nm, an increase of 30%; see Figure 4c). The interface interaction changes from one governed by the tip-substrate interaction to one governed by the mediating water layer.

This intercalated water layer improves the *quality* of contact at the tip/water/substrate interface. The intercalated water molecules act as pinning sites and increase the degree of interaction between the tip and sample, as evidenced by the change in RI[48]. The formation and growth of a water meniscus with increased humidity increases the number of molecules at the contact interface but separates the tip and substrate further (Figure 4c) to decrease the number of tip atoms directly in contact with the HOPG. The total number of water molecules in the tip-substrate area increases, as seen in Figure 3c,d. The contact quality also increases. We quantify the contact quality by multiplying the number of water molecules within 0.5 nm of both the tip and HOPG surface, *N*, by (1-RI), which we call the effective contact quality. The cutoff of 0.5 nm was chosen as it is slightly larger than the range of the water-graphite and water-tip potentials, thus capturing the first layer of water molecules. The value (1-RI) is used in this

calculation since RI approaches 0 and (1-RI) approaches 1 for energetically favorable sites of water adsorption. The higher the effective contact quality, the closer the positions of water molecules to the lower energy sites and/or the greater the number of water molecules at the interface that exist at low energy sites on substrate. As seen in Figure 3b, the effective contact quality increases steeply from 0 and 80% humidity, as water adsorbs onto the surface and intercalates into the contact. This trend agrees generally with the simulations of Müser and co-workers[51-52], who showed that isolated interfacial adsorbed molecules significantly increase friction for interfaces that otherwise would have low friction, *e.g.* incommensurate crystal lattices or interfaces with at least one amorphous material. While this mechanism has the same effect of increasing friction, it differs from the recent observation of increased contact quality due to the formation of interfacial covalent bonds[53-54] or from a sliding-induced increase of commensurability seen in flexible graphene samples[35]. Here, the water molecules are the driving component.

As humidity further increases from 80 to 100%, a thin water film covers the entire HOPG surface. This diminishes the effect of the Laplace pressure[24] but more importantly, reduces the contact quality due to more water molecules sitting at energetically unfavorable sites than at energetically favorable sites. As seen in Fig. 3b, above 80%, additional interfacial water molecules lower the effective contact quality. At this higher areal density, the interfacial water molecules interact more strongly with each other laterally, and form a densely-packed, partially ordered structure (shown in Figure S-9)[42]. Put simply, fewer molecules in preferential pinning sites reduces the degree to which they inhibit sliding, leading to lower friction.

At these high humidities, we observe the formation of a layer of water across the full HOPG surface, with lateral hexagonal order in the simulations with a radial distribution

reminiscent of hexagonal ice (see Figure S-9a)[42]. An ordered layer of ice due to confinement at an AFM tip-graphite interface has been previously claimed[28,29]. In our simulations and experiments, the periodicity of slips seen in both experiments and simulations does not change with humidity within error (see Figure S-2,5)[42], suggesting that this ice-like layer is slightly perturbed by the tip. The spontaneous formation of an ice-like monolayer and bilayer on the free surface of graphite from adsorbed water has been previously reported in MD simulations[33]. In our simulations, at high humidities, the ordered water resembles hexagonal ice across the majority of the surface outside the contact zone; however, that order is partially disrupted near the center of the tip-sample contact, as seen in Figure 3d. We suggest that this allows the HOPG lattice to determine the stick slip pattern.

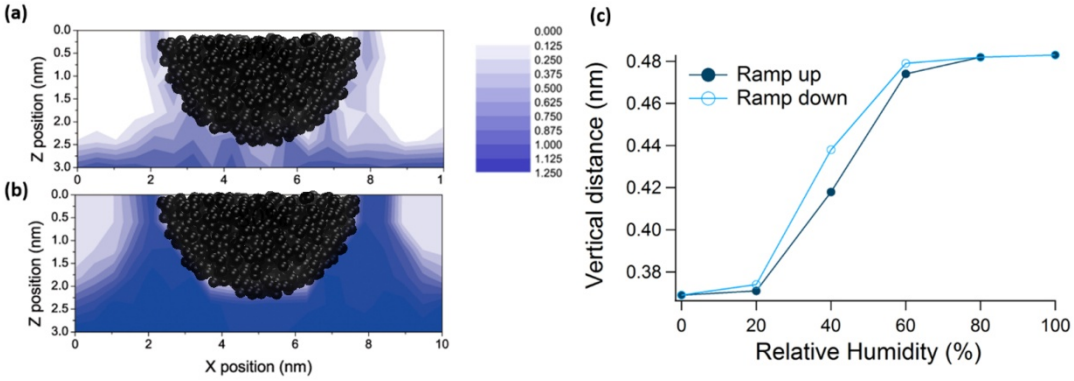

Figure 4: (a, b) Time-averaged density profiles of water molecules from simulations. At 40% RH the presence of a meniscus is evident. At 80% RH, the meniscus is more clearly developed. (c) Average minimum vertical distance between the bottommost tip atom and topmost substrate atoms at different humidities.

The friction force also shows hysteresis between ramping up and ramping down the relative humidity, with the peak friction occurring at a higher humidity while ramping up. Figures 2a and 3a show that this hysteresis can be seen in both experiments and simulations, though the hysteresis is more dramatic in the experiments. In experiments at 20% humidity, friction is 2.5x lower if the target humidity is reached by increasing the humidity as compared with decreasing the humidity; at 60% humidity, friction is 2.4x higher when measured after increasing *vs.* decreasing the humidity. If the sample is annealed in vacuum at 150 ^{o}C for 1 hour between each test at a different humidity in the experiments, intermediate behavior is seen (Figure 2b). The data points were not taken in the same ramping up/ramping down order as those in Figure 2a due to experimental limitations. However, multiple datasets were taken at 11-15%, 58%, and 76% RH after fresh anneals. One dataset for each of these humidities followed a set at lower humidity, while the other followed a higher humidity. The friction agrees within the scatter of the measurements for each dataset, thus demonstrating a lack of history dependence.

Vacuum annealing before setting the humidity at each desired level will remove most previously adsorbed water molecules from the HOPG surface. This suggests that the friction hysteresis comes from hysteresis in the adsorption and subsequent desorption of water molecules on the tip and substrate. This effect can be explained by considering that the energy barrier for adsorption of water on graphite surfaces is lower than that for desorption[55-56]. Previous experiments showed that there is an intrinsic hysteresis of water molecules' adsorption on different surfaces, including graphite, gold, and mica, when the relative humidity is increased and then decreased[57-58]. Our GCMC simulations tested for adsorption hysteresis by measuring the number of water molecules at a given humidity in steady state (see Figure S-10)[42]. We see a greater number of adsorbed molecules on the surface (within 0.5 nm of the substrate) when

ramping down the humidity in the simulations. For example, we observe 30% more water molecules on the surface at 60% humidity ramping down than when ramping up (see Figure S-10)[42]. Note that this implies that the short time window (~0.2 ns) within which the observed steady state is reached is not sufficient to enable all kinetic barriers to be traversed to reach the true equilibrium, for which no hysteresis should be observed; indeed, the time elapsed between different humidity levels in experiments, of the order of 1 hour, is not sufficient. Thus, the hysteresis of water adsorption causes the friction peak to shift to lower humidity when ramping the humidity down, as observed in both experiments and simulations. The adsorption hysteresis in experiments may also be affected by surface defects, which alter the accessibility of energetically favorable higher energy sites such as atomic steps[20]. However, the pristine surface used in the simulations does not involve any defects, potentially contributing to the difference in friction magnitude between experiments and simulations.

IV. Conclusions

AFM experiments and GCMC simulations were used to investigate the origins of humidity-dependent friction for the interfacial sliding of a ta-C tip on a HOPG substrate. We find in both experiments and simulations that water does not lubricate the interface, but rather it increases friction until a sufficient threshold humidity level is reached. Instead, a non-monotonic friction trend is observed in which the friction force first increases and then decreases as relative humidity increases. This trend appears as a peak with a 3-fold increase of friction from <1% humidity to the maximum value in experiments and a 6-fold increase in simulations. This non-monotonic trend is attributed to changes in the amount and location of adsorbed water at the interface. Low humidities show very sparse water coverage, so solid-solid contact between the tip and sample through van der Waals interactions dominate. Moderate humidities show

increased water adsorption at the tip-sample interface. The growing amount of interfacial water creates pinning sites across the interface, thus increasing friction, in agreement with prior general models for adsorbates[51-52]. At high humidities, we observe the formation of a meniscus and then a water film. However, the increasing distance between the tip and sample show that capillary adhesion is not the dominant effect driving the non-monotonic trend. Instead, the friction changes arise from changing contact quality due to intercalated water molecules. Specifically, lateral water-water interactions to form an ordered water film reduce the fraction of water molecules at sites with low registry index (*i.e.* pinning sites). This phenomenon is reminiscent of quartz crystal microbalance experiments showing that a partial film of adsorbates on a metal surface exhibit significant dissipation due to strong adsorbate-substrate interactions, but when a full monolayer is formed, lateral interactions de-pin the adsorbates from the substrate and dissipation is reduced[63-64].

In addition, for the first time, a humidity-dependent hysteresis in friction was observed in both experiments and simulations as a shift in the friction peak to higher humidity when ramping down vs. ramping up the relative humidity. The friction hysteresis was attributed to the intrinsic adsorption/desorption hysteresis of water molecules on surfaces due to the exothermic nature of adsorption (a higher energy barrier to desorption compared to adsorption). This shows that care must be taken when studying the humidity dependence of friction, as the history of water exposure may significantly affect the results obtained at a given humidity.

Our study provides atomic insights into the mechanisms underlying humidity-dependent friction and friction hysteresis on HOPG, although these mechanisms may also be active for other surfaces. These insights could potentially advance the development of nanoscale devices that need to operate in ambient conditions with varying humidity. These results contrast the well-

known decrease of friction (and wear) for graphite-based interfaces with increasing humidity observed the macroscale[6,7]. The macroscale results involve a multi-asperity contact, the breaking and reforming of bonds, wear, material transfer and removal, oxidation, and defect interactions. In particular, the poor macroscopic tribological behavior of graphite in dry or vacuum environments mirrors that of diamond and other hydrogen-free carbon-based systems[59], where dangling bonds formed during sliding create high friction unless they are passivated by the dissociative chemisorption of a sufficient quantity of water molecules from the vapor phase. None of these considerations are at play in these nanoscale investigations, as C-C bond breaking is avoided at the loads we use. The nature of water transport, diffusion, meniscus formation, and trapping of reservoirs will also be very different for a macroscopic multiple asperity contact compared to the simplified geometry of a single nanoscale contact. Our study suggests that, at the asperity level, in the absence of wear and material transfer, water will strongly affect friction in a manner that depends on the humidity and its history. In particular, the results suggest that the increase of friction due to adsorbates at the interface can be mitigated if the adsorbates have weak interactions with the interfacial materials to enable lateral diffusion and subsequent formation of adsorbate regions that are close enough to strongly interactions with each other and thus be prevented from serving as pinning sites. Further work is required to study intermediate length-scales to establish connections between nanoscale and macroscale behavior.

Acknowledgements: This work was funded by the U.S. National Science Foundation under CMMI-1401164 and CMMI-1362565. This work used the Extreme Science and Engineering Discovery

Environment (XSEDE), which was supported by National Science Foundation Grant No. ACI-1053575. K. Hasz was supported by the NSF GRFP.

Author Contributions: K.H. performed the experiments. Z.Y. conducted the simulations. All authors discussed and analyzed the results, and wrote the manuscript together.

Competing Interests: The authors declare that they have no competing financial interests.

Correspondence: Correspondence and requests for materials should be addressed to R.W.C. (email: carpick@seas.upenn.edu)

1. J.K. Lancaster, Tribol. Int. 23, 371–389 (1990).
2. Z. Chen, X. He, C. Xiao, and S. H. Kim, Lubricants, **6(3)**, 74 (2018).
3. M. B. Petersonand R. L. Johnson, Tech. Rep. (1953).
4. H. S. Khareand D. L. Burris, Tribol. Lett. **53**, 329–336 (2014).
5. G. Rowe, Wear **3**, 274–285 (1960).
6. R. H. Savage, J. Appl. Phys. **19**, 1–10 (1948).
7. R. H. Savageand D. L. Schaefer, J. Appl. Phys. **27**, 136 (1956).
8. A. R. Konicek,D. S. Grierson, P. U. P. A. Gilbert, W. G. Sawyer, A. V. Sumant, and R. W. Carpick, Phys. Rev. Lett. **100**, 235502 (2008).
9. D. Ramadanoff and S. W. Glass, Electr. Eng. 1944, **63,** 825–829 (1944).
10. J. Lepage, and H. Zaïdi, In Proceedings of the 14th Leeds-Lyon Symposium on Interface Dynamics; Dowson, D., Taylor, C.M., Godet, M., Berthe, D., Eds.; Elsevier: Amsterdam, The Netherlands, pp. 259–266 (1988).

11. A. Allouche, and Y. Ferro, Dissociative adsorption of small molecules at vacancies on the graphite (0001) surface. Carbon, **44**, 3320–3327 (2006).
12. P. Cabrera-Sanfelix and G. R. Darling, J. Phys. Chem. C, **111,** 18258–18263 (2007).
13. J. C. Rietsch, P. Brender, J. Dentzer, R. Gadiou, L. Vidal, and C. Vix-Guterl, Carbon, 55, 90–97 (2013).
14. C. Greiner, J. R. Felts, Z. Dai, W. P. King, and R. W. Carpick, ACS Nano **6**, 4305–4313 (2012).
15. M. Farshchi-Tabrizia, M. Kappl, and H.-J. Butt, J. Adhes. Sci. Technol. **22**, 181–203 (2008).
16. D. Sedin and K. Rowlen, Anal. Chem. **72**, 2183–9 (2000).
17. Z. Ye, P. Egberts, G. H. Han, A. T. C. Johnson, R. W. Carpick, and A. Martini, ACS Nano **10**, (2016).
18. M. He, A. Szuchmacher Blum, D. E. Aston, C. Buenviaje, R. M. Overney, and R. Luginbühl, J. Chem. Phys. **114**, 1355–1360 (2001).
19. X. Xiao and L. Qian, Langmuir **16**, 8153–8158 (2000).
20. L. Xu, A. Lio, J. Hu, D. F. Ogletree, and M. Salmeron, J. Phys. Chem. B **102**, 540–548 (1998).
21. M. Binggeli and C. M. Mate, Appl. Phys. Lett. **65**, 415–417 (1994).
22. D. B. Asay and S. H. Kim, J. Chem. Phys. **124,** 174712 (2006).
23. E. Riedo, F. Levy, and H. Brune, Phys. Rev. Lett. **88,** 185505 (2002).
24. D. B. Asay, M. P. de Boer, and S. H. Kim, J. Adhes. Sci. Technol. **24**, 2363–2382 (2010).
25. T. Rhee, M. Shin, and H. Jang, Tribol. Int. **94**, 234–239 (2016).

26. A. Schumacher, N. Kruse, R. Prins, E. Meyer, R. Luthi, L. Howald, H.-J. Guntherodt, and L. Scandella, J. Vac. Sci. Technol. B **14**, 1264 (1996).

27. R. W. Carpick, J. Batteas, and M. deBoer, Scanning Probe Studies of Nanoscale Adhesion Between Solids in the Presence of Liquids and Monolayer Films, 951–980 (Springer Berlin Heidelberg, Berlin, Heidelberg, 2007).

28. K. B. Jinesh and J. W. M. Frenken, Phys. Rev. Lett. **96**, 166103 (2006).

29. K. B. Jinesh and J. W. M. Frenken, Phys. Rev. Lett. **101**, 036101 (2008).

30. J. G. Vilhena, C. Pimentel, P. Pedraz, F. Luo, P. A. Serena, C. M. Pina, E. Gnecco, and R. Perez, ACS Nano **10,** (2016).

31. A. Opitz, S. I.-U. Ahmed, J. A. Schaefer, and M. Scherge, Surf. Sci. **504,** (2002).

32. Z. Li, Y. Wang, A. Kozbial, G. Shenoy, F. Zhou, R. McGinley, P. Ireland, B. Morganstein, A. Kunkel, S. P. Surwade, L. Li, and H. Liu, Nat. Mater. **12**, 925–31 (2013).

33. A. Akaishi, T. Yonemaru, and J. Nakamura, ACS Omega, **2(5)**, 2184-2190 (2017).

34. R. W. Carpick and M. Salmeron, Chem. Rev. **97**, 1163-1194 (1997).

35. S. Li, Q. Li, R. W. Carpick, P. Gumbsch, X.-Z. Liu, X. Ding, J. Sun, and J. Li, Nature **539**, 541-545 (2016).

36. F. Taherian, V. Marcon, N. F. A. Van Der Vegt, and F. Leroy, Langmuir **29**, 1457–1465 (2013).

37. Y.-C. Lin, C.-C. Lu, C.-H. Yeh, C. Jin, K. Suenaga, and P. Chiu, Nano Lett. **12**, 414–419 (2012).

38. J. E. Sader, J. W. M. Chon, and P. Mulvaney, Rev. Sci. Instrum. **70**, 3967–3969 (1999).

39. C. P. Green, H. Lioe, J. P. Cleveland, R. Proksch, P. Mulvaney, and J. E. Sader, Rev. Sci. Instrum. **75**, 1988–1996 (2004).

40. J. Villarrubia, J. Res. Nat. Inst. Stand. Technol. **102**, 425 (1997).

41. E. E. Flater, G. E. Zacharakis-Jutz, B. G. Dumba, I. A. White, and C. A. Clifford, Ultramicroscopy **146**, 130–143 (2014).

42. See Supplemental Material at (URL) for further details.

43. Y. Dong, Q. Li, and A. Martini, J. Vac. Sci. Technol. A **31**, 030801 (2013).

44. K. R. Hadley and C. McCabe, Mol. Simul. **38**, 671–681 (2012).

45. S. J. Stuart, A. B. Tutein, and J. A. Harrison, J. Chem. Phys. **112**, 6472–6486 (2000).

46. B. Albert, B. Guy, and D. Damidot, Cem. Conc. Res. **36**, 783–790 (2006).

47. S. Plimpton, J. Comput. Phys. **117**, 1–19 (1995).

48. O. Hod, Chem. Phys. Chem. **14**, 2376–2391 (2013).

49. C. Lee, Q. Li, W. Kalb, X.-Z. Liu, H. Berger, R. W. Carpick, and J. Hone, Science **328**, 76-80 (2010).

50. K. E. Ryan, P. L. Keating, T. D. Jacobs, D. S. Grierson, K. T. Turner, R. W. Carpick, and J. A. Harrison, Langmuir. **30** 2028-37 (2014).

51. G. He, M. H. Muser, and M. O. Robbins, Science **284**, 1650 (1999).

52. L. Wenning and M. H. Muser, Europhys. Lett. **54**, 693-9 (2001).

53. Q. Li, T. E. Tullis, D. Goldsby, and R. W. Carpick, Nature **480**, 233-236 (2011).

54. Y. Liu and I. Szlufarska, Phys. Rev. Lett. **109**, 186102 (2012).

55. M. Luna, J. Colchero, and A. M. Baro, J. Phys. Chem. B **103**, 9576– 9581 (1999).

56. L. S. Kocherlakota, B. A. Krajina, and R. M. Overney, J. Chem. Phys. **143**, 241105 (2015).

57. J. H. Thomas III, and S. P. Sharma, J. Vac. Sci. Technol. **13**, 549–551 (1976).

58. M. Luna, J. Colchero, A. Gil, J. Gomez-Herrero, and A. M. Baró, Appl. Surf. Sci. **157**, 393–397 (2000).

59. M. Gardos and B. Soriano, J. Mater. Res. **5**, 2599–2609 (1990).

60. V. Molinero and E. B. Moore, J. Phys. Chem. B **113**, 4008− 4016 (2009).

61. L. Darré, M. R. Machado, and S. Pantano, Wiley Interdiscip. Rev. Comput. Mol. Sci. **2**, 921-930 (2012).

62. R. W. Carpick, D. F. Ogletree, and M. Salmeron, Appl. Phys. Lett. **70**, 1548-1550 (1997).

63. J. Krim, D. H. Solina, and R. Chiarello, Phys. Rev. Lett. **66,** 181 (1991).

64. E. D. Smith, M. O. Robbins, and M. Cieplak, Phys. Rev. B **54**, 8252-60 (1996).